Title

Terrain attributes and forage productivity predict catchment-scale soil organic carbon stocks

Authors

Devine, Scott M
O'Geen, Anthony T
Liu, Han
et al.

Publication Date

2020-06-01

DOI

10.1016/j.geoderma.2020.114286

Peer reviewed

Geoderma 368 (2020) 114286

Contents lists available at ScienceDirect

Geoderma

journal homepage: www.elsevier.com/locate/geoderma

Terrain attributes and forage productivity predict catchment-scale soil organic carbon stocks

Scott M. Devine[a,*], Anthony T. O'Geen[a], Han Liu[a], Yufang Jin[a], Helen E. Dahlke[a], Royce E. Larsen[b], Randy A. Dahlgren[a]

[a] Department of Land, Air and Water Resources, University of California, Davis, CA 95616-8627, USA
[b] University of California Cooperative Extension, San Luis Obispo, CA 90001, USA

ARTICLE INFO

Handling Editor: Ingrid Kögel-Knabner

Keywords:
Soil organic carbon
Digital soil mapping
Remote sensing
Rangeland
Complex terrain
Forage productivity

ABSTRACT

Accurate assessments of soil organic carbon (SOC) stocks are needed at multiple scales given their importance to both local soil health and global C cycles. Rangelands cover 54% of California, representing a large stock of SOC, but existing SOC estimates are uncertain. To improve understanding of fine-resolution SOC stocks in complex terrain and provide guidance to rangeland SOC inventories, we grid-sampled 105 locations (21-m grid cells) at two depths (0–10 and 10–30 cm) in a 10-ha annual grassland catchment in California's Central Coast Range. Soils were analyzed for bulk density, coarse fragments, SOC and texture. Monthly aerial imagery was acquired by an unmanned aerial vehicle to compare surface reflectance during two contrasting years (wet vs. dry) to SOC stocks. We found that the 0–30 cm soil thickness held 3.64 ± 0.71 kg SOC m^{-2} (mean ± SD) with a range of 1.97–5.49 kg SOC m^{-2}. The 0–10 cm soil thickness stored 47% of the 0–30 cm SOC stock with SOC concentrations twice as high in the 0–10 cm layer (1.40 ± 0.38%) as in the 10–30 cm layer (0.71 ± 0.15% SOC). Multiple linear regression (MLR) models explained 50–57% of SOC variability at 0–30 and 10–30 cm, but only 25% of variability at 0–10 cm. Based on cross-validation tests, MLR outperformed spatial interpolation methods and Random Forest models, best explaining SOC stocks with five environmental covariates: wet-year greenness, mean curvature, elevation, insolation, and slope. Lower hillslope positions, concave landforms, and enhanced wet-year greenness were associated with more SOC, and explained 11%, 24%, and 31% of variability in 0–30 cm SOC stocks, respectively. This study demonstrates that the accuracy of regional-scale SOC mapping of California rangelands benefits from considering microclimatic and topographic controls at the catchment-scale, in addition to broader scale mineralogical and macroclimatic controls identified in previous SOC studies.

1. Introduction

Soil organic carbon (SOC) represents an important pool of terrestrial C, with global estimates of 755, 1408, and 2060 Pg in the upper 30, 100, and 200 cm, respectively (Batjes, 2016). California rangelands cover approximately 54% of California (FRAP, 2018) and are thus an important natural reservoir of SOC. There is active interest in developing more accurate inventories of SOC at the landscape scale to create a baseline for monitoring SOC change (Suddick et al., 2013). SOC estimates are available from the Soil Survey Geographic Database (SSURGO). However, for rangelands, as opposed to croplands, soil survey map units typically reflect relatively broad-scale trends, often with more than one major soil component included in each map unit (Soil Science Division Staff, 2017). Moreover, there is uncertainty about the sampling and analysis intensity that went into populating SSURGO SOC data, as has been shown in comparative SOC accounting studies (Homann et al., 1998; Galbraith et al., 2003; Thompson and Kolka, 2005; Domke et al., 2017).

Foothills surrounding the Central Valley and along the coastal regions, the typical environment of California annual rangelands, present a challenging environment to inventory SOC due to their topographic complexity. As reviewed and analyzed at the regional scale by Silver et al. (2010), 17 studies reported SOC data for California rangeland soils, but none sought to understand SOC patterns in complex terrain. Erosion-deposition influenced patterns of SOC in cultivated landscapes are well recognized and studied (Kirkels et al., 2014). However, greater erosional loss of SOC from summit and shoulder positions of cultivated land, compared to adjacent undisturbed grassland (Pennock et al., 1994), suggests that rangelands with persistent groundcover and protection from erosion (Salls et al., 2018) may have less pronounced

* Corresponding author.
E-mail address: smdevine@ucdavis.edu (S.M. Devine).

https://doi.org/10.1016/j.geoderma.2020.114286
Received 7 August 2019; Received in revised form 18 February 2020; Accepted 19 February 2020

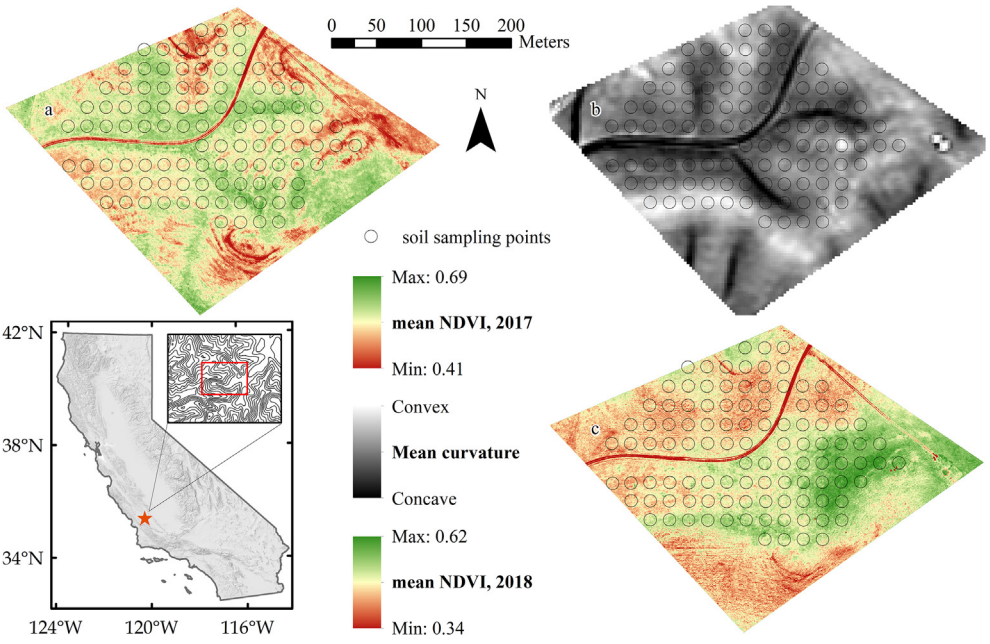

Fig. 1. Location of annual rangeland catchment (10 ha) in the eastern foothills of California's Central Coast Range with 21-m grid soil sampling scheme overlaying three terrain characteristics: (a) mean normalized difference vegetation index (NDVI) during the wet 2017 growing season; (b) mean curvature; and (c) mean NDVI during the dry 2018 growing season, all derived using unmanned aerial vehicle captured imagery.

hillslope SOC variation than reported in the agricultural literature.

Rigorous studies of catchment-scale SOC patterns in rangelands are only now beginning to emerge in semi-arid regions. In a 2.4 km^2 oak savannah watershed in southern Spain (mean precipitation = 582 mm yr^{-1}), researchers found that SOC stocks varied most closely with aspect, as north-facing sites had approximately twice the SOC as south-facing sites (Roman-Sanchez et al., 2018). The relationship of SOC to terrain curvature was only weakly expressed and the "noisy" SOC dataset was hypothesized to have partly arisen from past tree growth patterns concentrating C in the landscape, with only 18% of the variability explained in a 0–30 cm SOC validation test. Such oak tree enhancement of SOC within rangelands has been observed in California blue oak savanna where soils beneath oak trees contained ~50% more SOC stocks than adjacent grasslands (Dahlgren et al., 1997b). In contrast, a hillslope-scale study in a wetter (1400 mm yr^{-1}) Australian forested catchment found strong hillslope control with higher SOC in footslope positions and less SOC on steeper slopes (Hancock et al., 2010). Gessler et al. (2000) working on a southern California grassland transect at the hillslope scale found that lower landscape positions stored more SOC, especially in deeper soil layers. While progress has been made to quantify variations in SOC stocks across some California rangelands and in several uncultivated catchments around the world, additional studies are needed that consider the importance of integrated microclimate and hillslope processes on landscape-level SOC stocks.

Digital soil mapping studies offer a tool to improve mapping and understanding of SOC distribution. The approach uses statistical models to predict properties such as SOC from field- to watershed-, to national-scales (Minasny et al., 2013). Digital soil mapping incorporates two general statistical approaches that can also be combined in regression kriging to map SOC: (1) modeling spatial autocorrelation in SOC point measurements to interpolate point estimates; and/or (2) exploiting relationships between measured SOC and digitally available environmental covariates to create continuous estimates of SOC based on its relationship to covariates. Digital SOC mapping studies are typically able to explain 30–50% of the variation in SOC validation test datasets (Minasny et al., 2013), often exploiting a relationship between macroclimate and SOC at regional scales (Post et al., 1982) or across mountainous terrain, as has been observed in bioclimosequences in California (Jenny et al., 1968; Dahlgren et al., 1997a; Rasmussen et al., 2007; 2010). Only a fraction of SOC digital mapping studies have investigated SOC patterns at the small catchment scale using available environmental covariates (Minasny et al., 2013).

Complex terrain has diverse microclimates and forage productivity that varies at tens of meters (Devine et al., 2019), and this is expected to impact SOC stock patterns at catchment scale. Thus, understanding SOC distribution across these variable microclimates and landscape positions is needed to better predict climate change implications for landscape C storage. To address this knowledge gap, the objective of this study was to improve understanding of SOC patterns and its direct associations with terrain, remotely sensed surface reflectance, and vegetative productivity in a California annual grassland at the catchment scale using digital mapping techniques. We hypothesized greater SOC stocks in lower landscape positions, cooler microclimates (north to northwest facing), gentler slopes, and in concave positions, where hypothetically deeper soils exist, water converges for increased late season soil moisture supply, and higher annual productivity may supply greater organic matter inputs to organic carbon pools.

2. Methods

2.1. Study site description

The study site was located in a 10-ha annual grassland catchment with no perennial vegetation in San Luis Obispo County in the eastern foothills of California's Central Coast Range. Spanning 475–508 m elevation, the catchment lies 56 km inland from the Pacific Ocean within the county's lowest precipitation zone (Fig. 1) (Larsen et al., 2014). The Mediterranean climate consists of cool, wet winters (mean 1980–2010 January temperature = 7.9 °C) with sporadic precipitation from October-May (mean annual precipitation = 213 mm, site average over past 20 years), along with extended dry, hot summers (mean July temperature = 23.5 °C) (Daly et al., 2008). In the 2016–17 growing season (referred to as "wet year" or "2017"), 287 mm precipitation fell from October-April with a dry period in late February and March. In the 2017–18 growing season (referred to as "dry year" or "2018"), 123 mm precipitation fell with 60% in March and April. Growing season precipitation estimates were averages of three on-site tipping buckets.

The study site is an example of complex topography in California annual rangelands, including summit, shoulder, backslope, footslope, and concave-linear-convex surface curvatures with slopes ranging from 0 to 20° (Fig. 1). Catchment aspects were 45% south facing, 29% west

facing, 24% north facing, and 2% east facing (Liu et al., 2019). Soils formed from a mélange of sedimentary bedrock ranging from sandstones to shales. One soil map unit (Balcom-Nacimiento complex on 15–30% slopes) exists at the site with two major soil components described on backslope positions: Balcom (45% of map unit), a fine-loamy, mixed, superactive, thermic Typic Calcixerepts; and Nacimiento (30% of map unit), a fine-loamy, mixed, superactive, thermic Calcic Haploxerolls (Soil Survey Staff, 2003). The remaining 25% of the map unit is an assortment of 12 minor soil components, mostly described in other hillslope positions. Pedogenic calcium carbonate was observed throughout the site.

2.2. Soil sampling and analysis

We overlaid a 21-m sampling grid across the 10-ha catchment, producing a total of 115 sampling locations at the center of each 21-m grid cell. Ten locations on or within several meters of an unimproved road that dissected the catchment were excluded, so that 105 points were located with a Trimble Geo 7x Handheld Data Collector. Locations were refined with post-hoc differential correction to reduce location error to < 10 cm. A slide hammer coring device was used to collect one core at each location to 30-cm depth. The extracted cores were divided into 0–10 and 10–30 cm depths. Sampling depths were chosen to generally match rooting patterns of the annual species where SOC was expected to be concentrated (Gordon and Rice, 1992; Holmes and Rice, 1996).

Soil samples were air-dried, gently crushed, and passed through a 2-mm sieve. Coarse fragment mass was quantified and when coarse fragment mass exceeded 5% of the sample mass, coarse fragment volume was determined using liquid displacement. Soils were then corrected for coarse fragment mass and volume to calculate bulk density on a fine-earth fraction basis (≤2 mm) (Dane and Topp, 2002). Soil texture was determined using the hydrometer method following shaking with Na-hexametaphosphate (Gavlak et al., 2005). Gravimetric water content was determined on soil samples dried overnight at 105 °C. Visible, fine roots were removed from 30 to 40 g subsamples of the 2-mm sieved soil. These subsamples were finely ground in rolling cylinders with stainless-steel ball bearings to pass a 180-μm sieve. To determine SOC, carbonates were first removed with HCl (Midwood and Boutton, 1998) from 100 to 150 mg subsamples of ground soil. Carbonate removal was accomplished by first adding 1 mL of 0.1 M HCl to each subsample (no shaking) and letting the sample sit overnight. Additional 0.3 mL aliquots of 1 M HCl were added each day until reaction completion was verified using pH indicator paper (pH < 4–5). Finally, residual acid was removed by drying at 60 °C for 72 h, so that dissolved organics in the supernatant were retained within the acidified soil. Organic C and total N were determined on subsamples of finely ground acidified soils by dry combustion (ECS 4010, Costech Analytical Technologies, Valencia, CA). Additionally, total C and N analysis were determined on subsamples of finely ground, untreated soil. Sample mass corrections from carbonate removal were deemed unnecessary, since the HCl carbonate removal method results in a negligible change in sample mass. Comparison of total N concentrations in acidified and untreated samples were not significantly different as assessed by a paired *t*-test for each depth (0–10 cm: $p = 0.38$; 10–30 cm: $p = 0.89$), verifying the efficacy of this approach. Soil carbon stock was calculated as follows:

$$\mathrm{kg\,SOC\,m^{-2}} = \%\,\mathrm{SOC} \times \mathrm{BD} \times (1-\mathrm{CF}) \times \frac{Z}{10} \quad (1)$$

where BD = bulk density in g $\mathrm{cm^{-3}}$, CF = coarse fragments volumetric fraction (> 2 mm), and Z = horizon thickness in cm.

2.3. UAV flights and reflectance data

A 3DR Solo quadcopter (UAV), equipped with a MicaSense RedEdge camera (MicaSense Inc., Seattle, WA; five spectral bands: blue (465–485 nm), green (550–570 nm), red (663–673 nm), red-edge (712–722 nm), and near-infrared (820–860 nm) (NIR)), was used for ten flights over the 10-ha catchment during the growing season for the two years (Liu et al., 2019). Six flights were made from November 11, 2016 to April 30, 2017, and four from January 18, 2018 to April 14, 2018. Further details about flight plans and image processing to produce illumination-corrected red and NIR reflectance values used to calculate normalized difference vegetation index (NDVI) at 30-cm resolution are available in Liu et al. (2019).

Mean growing season NDVI, red, red-edge, and NIR values, as opposed to individual monthly reflectance data, were used in statistical models to reduce the number of correlated covariates considered. For example, within both the wet (2017) and dry (2018) years, monthly NDVI was significantly correlated across all months (except for January) at the soil sampling locations (2017: $p < 0.001$; $0.14 < R^2 < 0.68$; 2018: $p < 0.001$; $0.38 < R^2 < 0.81$). Thus, 2017 and 2018 NDVI growing season averages were used as model inputs as opposed to monthly data. Reflectance values for the soil sampling locations were estimated using the *extract* function from the *raster* package in R (Hijmans, 2017), taking the mean value of all 30-cm pixels within a 1-m buffer of the soil sample location.

2.4. Catchment terrain characteristics

We created a 1.86-cm resolution digital surface model (DSM) over the study area, using photogrammetry from UAV imagery captured on March 9, 2017 (Liu et al., 2019), and then derived terrain characteristics using ArcGIS Desktop 10.5 software. Effects of low, herbaceous vegetation were minimal (mean height = 7 cm on February 15, 2017, and 14 cm on March 15, 2017) and therefore not considered in the analysis. Seven ground control points showed a mean RMSE of 6 cm in georegistration (all dimensions). These high resolution data were aggregated to 30-cm pixel size by calculating the mean value of all pixels within this coarser grid, using the ArcGIS aggregate function (Spatial Analyst: Generalization: Aggregate). The 30-cm grid was then filtered to smooth anomalies using the ArcGIS default low pass filter function (Spatial Analyst: Neighborhood: Filter). Data were further aggregated to 3-m and filtered again using the same approach before calculating elevation, slope, aspect, curvature (profile, plan, and mean), and annual clear sky solar radiation (insolation), using ArcGIS Spatial Analyst tools. The aggregating and filtering process to 3-m resolution was deemed necessary to produce stable estimates of terrain curvature, whereas estimates of elevation, slope, and aspect were strongly correlated with estimates from the 30-cm resolution DSM ($R^2 > 0.99$). Another DSM produced from November 2016 drone imagery showed $R^2 > 0.98$ for comparisons of elevation, slope, and insolation, and $R^2 = 0.91$–0.94 for comparisons of curvature (mean, plan, and profile) ($n = 105$).

2.5. Vegetation monitoring

We clipped standing forage within 0.09 $\mathrm{m^2}$ quadrats four times in each growing season, approximately one month apart. In 2017 at each date, 34 locations were clipped within the soil sampling grid, while in 2018 at each date, 16 locations were clipped. Forage was oven dried at 60 °C for 48 h before weighing. We recorded grass and forb height and species composition using the dry-weight rank method (Ratliff and Frost, 1990) as previously reported in Devine et al. (2019). Gradients in annual forage production are diffuse across the study catchment; there are no shrubs or perennial grass patches creating islands of enhanced soil quality as found in several semi-arid and arid ecosystems such as Mediterranean oak woodlands (Dahlgren et al. 1997b). Peak standing biomass and modeled SOC at forage sampling locations were compared as an additional test of the relationship between aboveground productivity and SOC stocks.

2.6. Statistical modeling

Least-squares regression and rank order correlation (Spearman) tests were first used to examine associations among soil properties, terrain characteristics, and surface reflectance and to guide selection of a set of important environmental covariates for mapping SOC stocks and understanding controls on SOC distribution without suffering from excessive collinearity. Spatial autocorrelation of least-square regression residuals was tested to check independence of error terms as an assumption in evaluating regression coefficient error estimates. Profile and plan curvature were eliminated before model testing because of high correlation with mean curvature ($R^2 > 0.9$). Mean growing season red-edge reflectance was eliminated from modeling because of high correlation with NIR reflectance (2017: $R^2 = 0.70$; 2018: $R^2 = 0.83$). Similarly, mean growing season red reflectance was eliminated from modeling because of its high correlation with NDVI (2017: $R^2 = 0.80$; 2018: $R^2 = 0.63$). This narrowed the pool of environmental covariates considered in statistical models to: (1) elevation; (2) slope; (3) insolation; (4) mean curvature; (5) $NDVI_{2017}$; (6) $NDVI_{2018}$; (7) NIR_{2017}; and (8) NIR_{2018}.

Model selection for understanding SOC patterns in the catchment and SOC mapping was performed using a k-fold cross-validation approach that considered all 255 possible combinations of the eight environmental covariates selected for analysis[1]. We tested all 255 possible variable subsets using multiple linear regression (MLR) and Random Forest to model 0–10 cm, 10–30 cm, and 0–30 cm SOC datasets. The cross-validated root mean square error was calculated for each predictor subset and modeling approach combination:

$$\text{cross validated RMSE}_k = \frac{1}{k}\sum_{i=1}^{k} \text{RMSE}_i \quad (2)$$

where RMSE is the root mean square error of each i^{th} fold out-of-bag dataset of size n (in our case either 5 or 6, since the 105 points were divided into 20-folds) calculated as:

$$\sqrt{\frac{1}{n}\sum_{i=1}^{n} (\text{predicted}_i - \text{observed}_i)^2} \quad (3)$$

The proportion of variance explained (R^2) was also tabulated during the cross-validation process. For each Random Forest model iteration, the *tuneRF* function was used to set the *mtry* argument during the call to *randomForest* in the *randomForest* package in R (Liaw and Wiener, 2002; R Core Team, 2018). The *mtry* argument defines the number of variables available for splitting at each tree node.

Spatial interpolation methods, including nearest neighbor averaging, inverse distance weighting, and ordinary kriging, the latter a common approach in digital soil mapping (Keskin and Grunwald, 2018), were compared to MLR and Random Forest in cross-validation tests as benchmarks for modeling and mapping SOC stocks. Our objective was to evaluate the accuracy of a catchment scale map created by leveraging only the soil point SOC data and spatial autocorrelation, without any of the finer scale covariate information available to the MLR and random forest modeling approaches. In this exercise, for each of the three spatial interpolation approaches, a SOC map was created within each k-fold from 99 or 100 points, with prediction of the out-of-bag 5 or 6 samples contributing to the overall cross-validation statistic of all 20 k-folds. These spatial averaging techniques were implemented with a call in R software to *gstat*. Ordinary kriging was implemented with additional calls to *variogram* and *fit.variogram*, all in the *gstat* package (Pebesma, 2004; Graler et al., 2016), which allowed for consideration of five different variogram models and a range of kappa values during variogram model optimization in each k-fold on-the-fly. Finally, a null model was tested wherein each k-fold the mean of 99 or 100 observations served as the prediction for 5 or 6 out-of-bag observations.

The overall best model was defined as the model that had the lowest cross-validated RMSE. Since the best models turned out to be MLR, four diagnostic plots produced by *plot(lm_object)* were examined to check goodness-of-fit and verify appropriateness of a linear modeling approach for understanding associations between SOC and environmental covariates. Variance-inflation factors were calculated using the *vif* function and partial regression plots ('added-variable' plots) were checked using the *avPlots* function, both from the *car* package in R software (Fox and Weisberg, 2011). To better understand the relative importance of environmental covariates in explaining SOC variability, R^2 from the best MLR model was decomposed into estimates of each individual regressor's contribution, using the *calc.relimp* function from the *relaimpo* package and the recommended *lmg* metric in R software (Groemping, 2006).

Spatial autocorrelation in soil properties and linear regression residuals was tested using a Monte-Carlo approach with the *moran.mc* function from the *spdep* package in R software (Bivand and Wong, 2018) as follows. First, Moran's I was calculated for each variable of interest (SOC concentrations (%) and stocks (kg m^{-2}), bulk density, particle size fractions, and linear regression residuals). Then, each variable of interest or model residuals had its point estimates randomly reassigned across the catchment to the 105 sampled locations an additional 999 times, and Moran's I was recalculated each time. Autocorrelation p values reflect a ranking of actual observed Moran's I relative to these random permutations, and thus, provide an approximate probability that the variable's or linear regression residuals' observed spatial autocorrelation was produced by chance alone. If the original spatial autocorrelation in the soil property of interest has been accounted for by spatial autocorrelation in the model's explanatory variables, then the residuals should show no spatial autocorrelation. Moreover, lack of linear regression residual spatial autocorrelation suggests that regression kriging (e.g. combining MLR with kriging of residuals) would not add to the model's predictive power.

3. Results

3.1. Terrain properties

The 105 sample locations captured a range of topographic characteristics within a relatively narrow elevation band of 475–508 m. Landforms ranged from concave to linear to convex, slopes from 0.3 to 23.3°, clear sky radiation (insolation) from 1067 to 1471 kWh m^{-2} yr^{-1}, and mean growing season NDVI from 0.34 to 0.69 across the two study years (Table 1). Concave sites tended to be at lower elevation and greener in the wet year (Table 2). Higher elevation sites tended to have less clay and were greener in the dry year (Table 2). North-facing slopes tended to be steeper and south-facing slopes gentler (Table 2).

3.2. Soil properties

Across the catchment, the 0–30 cm soil layer held 3.64 ± 0.71 kg SOC m^{-2} (mean ± SD) with a range of 1.97–5.49 kg SOC m^{-2} (Table 1). SOC was more concentrated near the surface with the 0–10 cm depth containing 47% of the total 0–30 cm SOC and having twice the average SOC (1.40 ± 0.38%) of the 10–30 cm depth (0.71 ± 0.15%) (Table 3). Soils were predominantly loams, clay loams, and sandy loams, and particle size decreased with depth. There was 21 ± 4% clay in the 0–10 cm layer and 25 ± 6% clay in the 10–30 cm layer (Table 3). Bulk density and pH increased with depth and were significantly greater in the 10–30 cm layer (Table 3).

[1] See https://github.com/smdevine/CamattaCarbon/blob/master/publication/soilC_model_comparisons.R

Table 1
Statistics for 0–30 cm soil carbon and terrain properties from 3-m digital surface model at the points sampled in April 2018 (n = 105).

Stat.	SOC %	kg m^{-2}	BD g cm^{-3}	Curv. m^{-1}	Insol. kWh m^{-2}	Elev. m	Slope deg.	$NDVI_{2017}$	$NDVI_{2018}$
Min.	0.44	1.97	1.18	−1.77	1067	474.9	0.2	0.41	0.34
Q_1	0.81	3.16	1.27	−0.52	1270	486.8	9.0	0.56	0.42
Q_2	0.93	3.64	1.35	0.03	1355	491.8	11.6	0.60	0.46
Mean	0.92	3.64	1.34	0.08	1337	492.2	11.6	0.59	0.46
Q_3	1.03	4.15	1.40	0.50	1440	497.7	13.6	0.63	0.51
Max.	1.47	5.49	1.54	2.54	1471	507.9	23.3	0.69	0.62
SD	0.18	0.70	0.08	0.93	113	7.9	4.4	0.05	0.06

SOC = soil organic carbon; BD = bulk density; Curv = mean curvature; Elev = elevation; Insol = annual clear sky insolation (kWh m^{-2}); NDVI = Normalized difference vegetation index during 2017 (wet) and 2018 (dry) growing seasons; *Min.* = minimum; Q_1 = lower quartile (25th percentile); Q_2 = median; Q_3 = upper quartile (75th percentile); *Max.* = maximum; SD = standard deviation

Table 2
Spearman rank correlation coefficients for soil organic carbon (SOC) stocks at all depths, select 0–30 cm soil properties, terrain characteristics, and remote sensing information from two growing seasons (2017, a wet year, and 2018, a dry year) captured from an unmanned aerial vehicle. Values shown in **bold** were significant at α = 0.001 level. Values shown in *italic* were significant at α = 0.01 level (n = 105).

	$SOC_{0\text{-}30}$	$SOC_{0\text{-}10}$	$SOC_{10\text{-}30}$	$Clay_{0\text{-}30}$	$BD_{0\text{-}30}$	Elev.	Curv.	Insol.	Slope	$NDVI_{2017}$	$NDVI_{2018}$	NIR_{2017}
$SOC_{0\text{-}30}$	1											
$SOC_{0\text{-}10}$	**0.84**	1										
$SOC_{10\text{-}30}$	**0.82**	**0.43**	1									
$Clay_{0\text{-}30}$	**0.40**	NA	NA	1								
$BD_{0\text{-}30}$	0.06	NA	NA	−0.16	1							
Elev.	**−0.33**	−0.18	**−0.42**	**−0.44**	0.01	1						
Curv.	**−0.52**	*−0.27*	**−0.60**	−0.21	−0.17	**0.48**	1					
Insol.	−0.23	−0.08	**−0.33**	−0.23	0.06	−0.11	0.11	1				
Slope	−0.09	*−0.25*	0.11	0.20	−0.13	−0.17	−0.15	**−0.43**	1			
$NDVI_{2017}$	**0.53**	**0.40**	**0.46**	*0.27*	0.06	−0.14	**−0.36**	−0.01	*−0.29*	1		
$NDVI_{2018}$	0.08	0.11	0.01	*−0.30*	0.22	**0.58**	0.11	**−0.47**	−0.22	0.15	1	
NIR_{2017}	**0.29**	0.16	*0.30*	**0.39**	−0.09	**−0.54**	*−0.28*	0.17	−0.03	**0.55**	**−0.39**	1
NIR_{2018}	**−0.28**	−0.06	**−0.43**	**−0.34**	0.21	*0.31*	*0.28*	**0.39**	*−0.26*	**−0.37**	0.17	*−0.28*

SOC = soil organic carbon (kg m^{-2}); Elev = elevation (m); Curv = mean curvature; Insol. = annual clear sky insolation (kWh m^{-2}); NDVI = mean normalized difference vegetation index during a wet (2017) or dry (2018) growing season; NIR = mean near-infrared during a wet (2017) or dry (2018) growing season

Table 3
Soil properties for two depths sampled at the study catchment in April 2018 (n = 105). A paired *t*-test was used to compare difference in 0–10 and 10–30 cm soil properties.

Depth	Stat.	SOC	SOC	TN	Clay	Sand	Silt	BD	pH	CF
		kg m^{-2}	%————					g cm^{-3}		%
0–10 cm	*Min.*	0.81	0.72	0.08	10	26	12	0.83	7.3	0
	Q_1	1.40	1.18	0.13	19.2	34.8	34	1.15	7.7	0
	Q_2	1.70	1.35	0.15	22	38	38	1.24	7.8	0
	Mean	1.70	1.40	0.16	21.4	41.5	37.1	1.24	7.76	0.7
	Q_3	1.98	1.61	0.18	24	44.4	42.4	1.35	7.8	0.8
	Max.	3.28	3.08	0.37	30.8	76.8	50	1.75	8	9.9
	SD	0.41	0.38	0.04	4.3	10.4	7.7	0.16	0.11	1.5
10–30 cm	*Min.*	0.86	0.33	0.04	12	18	10	1.19	7.7	0
	Q_1	1.67	0.62	0.07	22	31.2	34	1.32	7.9	0
	Q_2	2.00	0.73	0.08	25.6	35.2	38	1.37	8	0
	Mean	1.93	0.71	0.08	25.0	38.5	36.4	1.38	7.95	1.9
	Q_3	2.22	0.80	0.09	28.4	43.6	42	1.43	8	1.8
	Max.	2.95	1.20	0.12	38	74.8	52	1.63	8.5	18.8
	SD	0.42	0.15	0.01	5.6	12.1	8.0	0.09	0.13	3.6
t-test	*p*	NA	< 0.001	< 0.001	< 0.001	< 0.001	0.18	< 0.001	< 0.001	0.002

SOC = soil organic carbon; TN = total nitrogen; BD = bulk density; CF = coarse fragments; *Min.* = minimum; Q_1 = lower quartile (25th percentile); Q_2 = median; Q_3 = upper quartile (75th percentile); *Max.* = maximum; SD = standard deviation, p = p value

3.3. Relationship of SOC to terrain properties, vegetation productivity, and soil texture

The 0–30 cm SOC stocks were significantly related to vegetation productivity e.g., mean growing season NDVI in 2017 (wet-year NDVI; R^2 = 0.31, $p < 0.001$), and several terrain properties, including mean curvature (R^2 = 0.24, $p < 0.001$) and elevation (R^2 = 0.11, $p < 0.001$). In contrast, there was no detectable association of 0–30 cm SOC stocks with mean NDVI in 2018 (dry-year NDVI), slope, or aspect, as represented by insolation (Fig. 2). Lower hillslope positions in the catchment tended to be concave, have more clay, higher NDVI, and greater SOC stocks (Table 2). The direct associations between terrain characteristics and SOC were generally stronger for the 10–30 cm layer compared to the 0–10 cm layer, except for the relationship with slope, which was strongest for the 0–10 cm layer (Table 2).

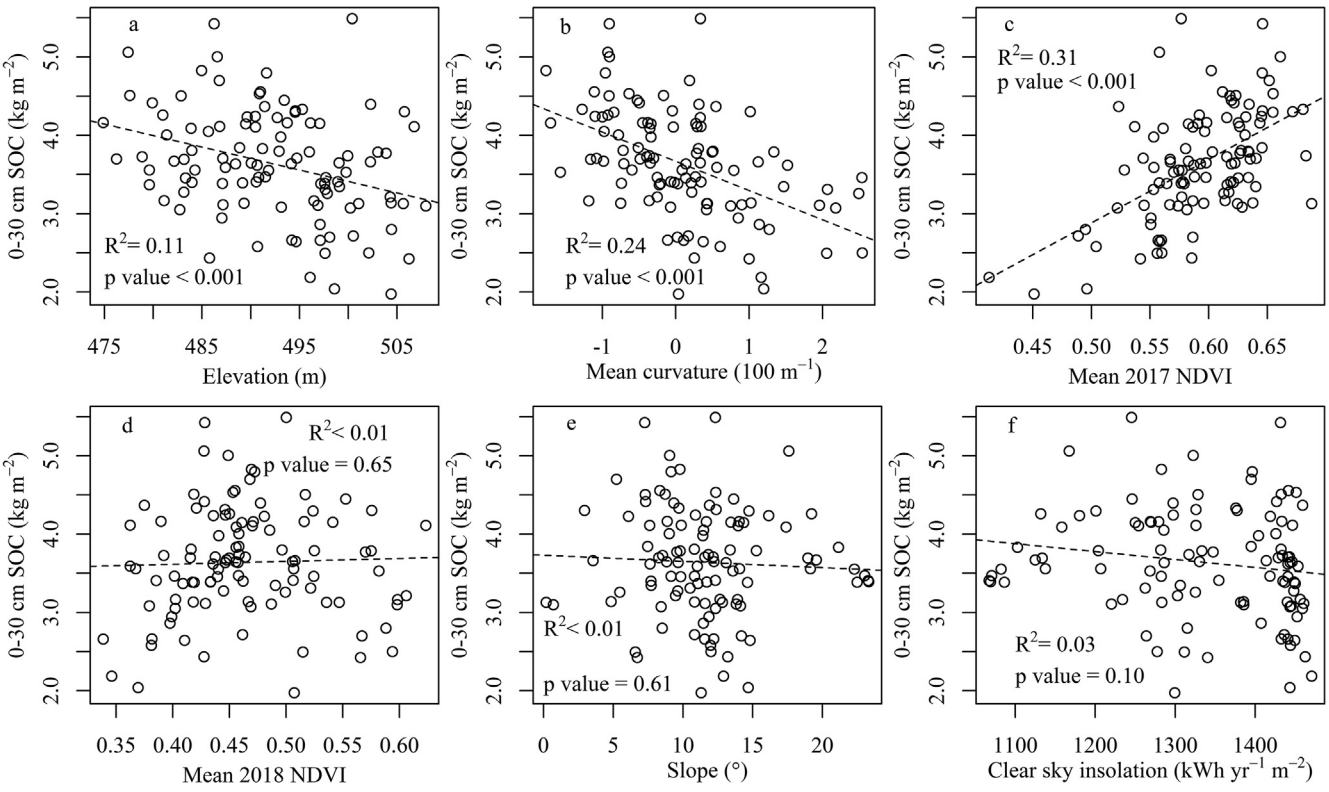

Fig. 2. a–f: Direct association between 0-30 cm soil organic carbon (SOC) and terrain characteristics derived from a 3-m digital surface model and mean normalized difference vegetation index (NDVI) during the (c) wet 2017 and (d) dry 2018 growing seasons.

3.4. Modeling and mapping SOC stocks

After rejecting the most collinear predictors, eight environmental covariates derived from UAV flights were considered to explain SOC stock patterns in the catchment. MLR models achieved maximum explanatory power with five variables and consistently outperformed Random Forest in 20-fold cross-validation tests at all depths (Tables 4 and 5). MLR models also outperformed various spatial interpolation techniques in 20-fold cross-validation tests with ordinary kriging performance comparable to simpler methods of spatial interpolation (Table S1). A MLR model that included mean curvature, slope, elevation, insolation, and wet-year NDVI explained 50% of variability in 0–30 cm SOC stocks across the catchment (20-fold cross-validated R^2 = 0.44) (Fig. 3). This five-variable MLR model outperformed the best Random Forest model (20-fold cross-validated R^2 = 0.36) with a mean cross-validated RMSE that was 6% lower (Table 5). Coefficients for this model using standardized predictors were all significant (α = 0.05), and their signs (positive vs. negative) met intuitive expectations (Table 4).

Importance metrics suggest that wet-year NDVI and curvature were responsible for 70% of explained variability. Even though slope and insolation had the largest normalized coefficients in this model

Table 4
Best performing multiple linear regression (MLR) and Random Forest models of 0–30 cm soil organic carbon (SOC) from one up to eight possible predictors, by number of predictors, selected from 20-fold cross-validation (CV) tests on all 255 possible subsets of eight predictors. Coefficient estimates for normalized covariate predictors ($(x_i - \bar{x})/sd$) are shown through five possible predictors, the best identified number and selection of covariates.

Covariates considered	Best MLR models	CV RMSE	CV R^2
	Predictors in best performing models	*kg m^{-2}*	
1	0.39*$NDVI_{2017}$	0.549	0.27
2	0.31*$NDVI_{2017}$ + −0.24*curvature	0.521	0.37
3	0.31*$NDVI_{2017}$ + −0.23*curvature + −0.11*insolation	0.511	0.38
4	0.31*$NDVI_{2017}$ + −0.19*curvature + −0.12*insolation + -0.10_{NS}*elevation	0.497	0.40
5	0.23*$NDVI_{2017}$ + −0.23*curvature + −0.28*insolation + −0.17*elevation + −0.25* slope	0.478	0.44
6	elevation, slope, insolation, curvature, $NDVI_{2017}$, NIR_{2018}	0.482	0.43
7	elevation, slope, insolation, curvature, $NDVI_{2017}$, NIR_{2017}, NIR_{2018}	0.491	0.42
8	All predictors	0.499	0.41
	Best Random Forest models		
2	curvature, $NDVI_{2017}$	0.533	0.33
3	curvature, $NDVI_{2017}$, $NDVI_{2018}$	0.523	0.33
4	elevation, curvature, $NDVI_{2017}$, $NDVI_{2018}$	0.510	0.36
5	elevation, insolation, curvature, $NDVI_{2017}$, $NDVI_{2018}$	0.513	0.36
6	elevation, slope, curvature, $NDVI_{2017}$, $NDVI_{2018}$, NIR_{2017}	0.519	0.33
7	elevation, slope, insolation, curvature, $NDVI_{2017}$, $NDVI_{2018}$, NIR_{2017}	0.523	0.32
8	All predictors	0.529	0.34

RMSE = root mean square error; NS = not significant (α = 0.05 level); insolation = annual clear sky insolation; NDVI = mean normalized difference vegetation index during a wet (2017) or dry (2018) growing season; NIR = mean near-infrared during a wet (2017) or dry (2018) growing season.

Table 5
Best performing multiple linear regression (MLR) and Random Forest models of 0–10, 10–30, and 0–30 cm soil organic carbon (SOC) selected from all 255 different combinations of 8 predictor variables in 20-fold cross validation (CV) tests. Best performing was defined as the simplest model to achieve the lowest mean RMSE during CV. Best models all had 4 or 5 predictors.

Best MLR models			
Depth *-cm-*	Predictors in best performing model	CV RMSE $kg\ m^{-2}$	CV R^2
0–10	elevation, slope, insolation, curvature, $NDVI_{2017}$	0.352	0.16
10–30	elevation, insolation, curvature, $NDVI_{2017}$, NIR_{2017}	0.264	0.53
0–30	elevation, slope, insolation, curvature, $NDVI_{2017}$	0.478	0.44
Best Random Forest models			
0–10	elevation, slope, insolation, $NDVI_{2017}$, $NDVI_{2018}$	0.354	0.16
10–30	curvature, $NDVI_{2018}$, NIR_{2017}, NIR_{2018}	0.287	0.46
0–30	elevation, curvature, $NDVI_{2017}$, $NDVI_{2018}$	0.510	0.36

NDVI = mean normalized difference vegetation index during a wet (2017) or dry (2018) growing season; NIR = mean near-infrared during a wet (2017) or dry (2018) growing season

(Table 4), importance metrics suggest they were only responsible for 17% of explained variability. Variance-inflation factors (VIF) showed that insolation (VIF = 2.75) and slope (VIF = 2.19) suffered from some collinearity (Table 2) in this model, which may inflate coefficient estimates. The other three covariates had lower VIFs ranging from 1.43 to 1.46. Indeed, the best two-variable MLR model using mean curvature and wet-year NDVI performed almost as well as the five-variable model, with its cross-validated RMSE only 0.04 kg m^{-2} higher and full dataset R^2 = 0.41 (Fig. 4; Table 4). Residuals from the two- and five-variable MLR models showed no strong evidence of spatial autocorrelation (Table 6).

Similar to the stronger direct associations between 10-30 cm SOC stocks and terrain characteristics compared to 0–10 cm SOC stocks (Table 2), the best MLR model explained the 10–30 cm layer SOC stock variability better (R^2 = 0.57 full dataset) than the 0–10 cm SOC stock variability (R^2 = 0.25 full dataset) (Table 5). Even though there was a contrasting performance for each depth, subsets of predictors in the best model for each depth were similar (Table 5). However, based on relative importance metrics for the best models, the dominant associations were different: slope and wet-year NDVI were responsible for 67% of explained variance in 0–10 cm SOC stocks, while wet-year NDVI and mean curvature were responsible for 65% of explained variance in 10–30 cm SOC stocks, the latter very similar to the 0–30 cm analysis. Insolation was more important to accuracy of the 10–30 cm model, responsible for 16% of explained variance in 10–30 cm SOC stocks compared to 7% of explained variance in 0–10 cm SOC stocks.

Given strong spatial autocorrelation in SOC stocks (Table 6), it was surprising that spatial interpolation techniques had relatively limited predictive power, compared to MLR and Random Forest approaches (Table S1). Ordinary kriging of 0–30 cm SOC stocks only produced a 20-fold cross-validated R^2 = 0.15. Kriging accuracy was higher for the 10–30 cm layer (R^2 = 0.26), and much lower for the 0–10 cm layer (20-fold cross-validated R^2 = 0.03; p = 0.07). Autocorrelation was stronger in the 10–30 cm layer compared to the 0–10 cm layer, which explains why ordinary kriging performed better for this layer. Regression kriging added no explanatory power to the MLR model, because residuals from the best MLR models showed no clear evidence of spatial autocorrelation (Table 6).

3.5. Relationship of estimated SOC to peak aboveground biomass

The best MLR model identified in cross-validation tests was used to map SOC stocks in the catchment (Fig. 5a). From this map, SOC values were extracted at points where aboveground biomass was sampled to compare how SOC stocks related to peak standing forage in strongly

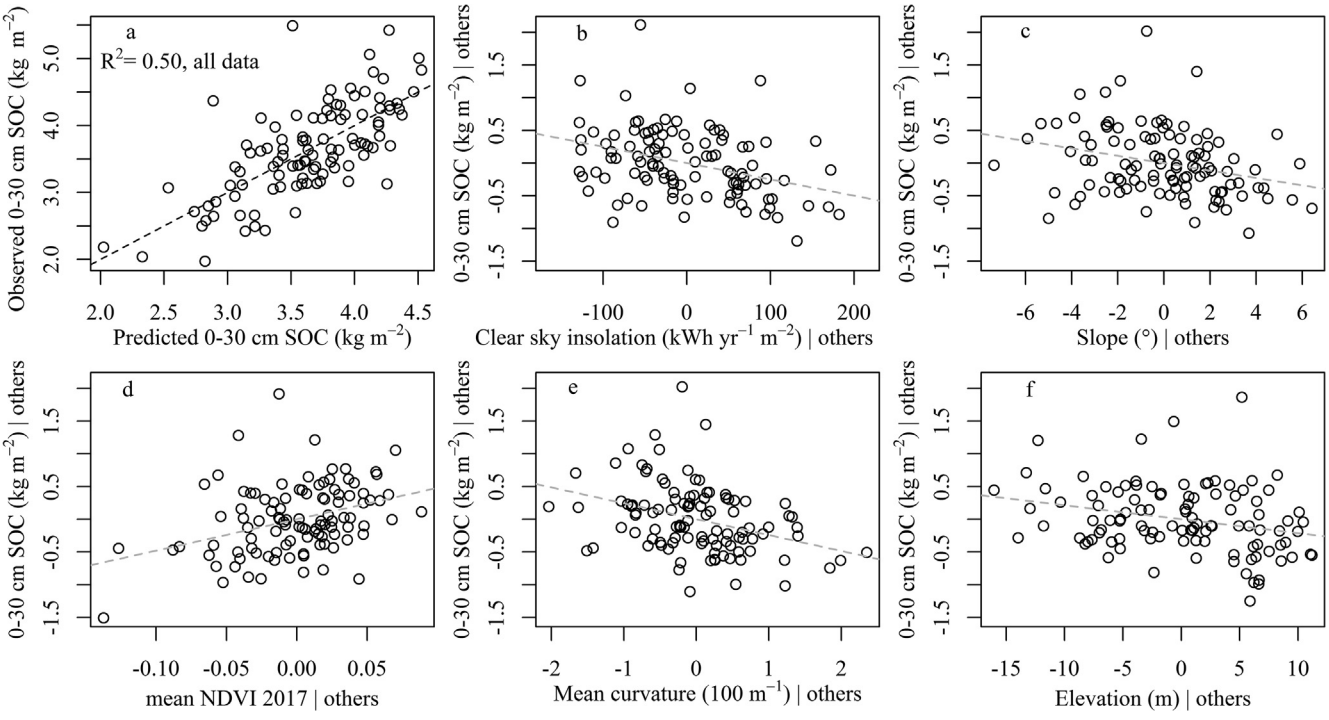

Fig. 3. a–f: Best 0–30 cm soil organic carbon (SOC) model identified during cross-validation, showing (a) Observed vs. predicted SOC and 1:1 line (black) and added-variable (aka 'partial regression') plots for each of the 5 predictors (x-axes) in this multiple linear regression best model: (b) Annual clear sky insolation; (c) Slope; (d) mean normalized difference vegetation index (NDVI) in 2017; (e) mean curvature; and (f) elevation. Each plot shows the relative contribution of the predictor to explaining variance in SOC after accounting for the other predictors' explanatory power in the model. Gray lines show the best-fit for each partial regression plot. The slopes of these gray lines are equal to the explanatory variables' beta coefficients in the overall MLR model, all very similar in magnitude and with p < 0.004 (Table 4). The meaning of "| others" is "after accounting for the other predictor variables."

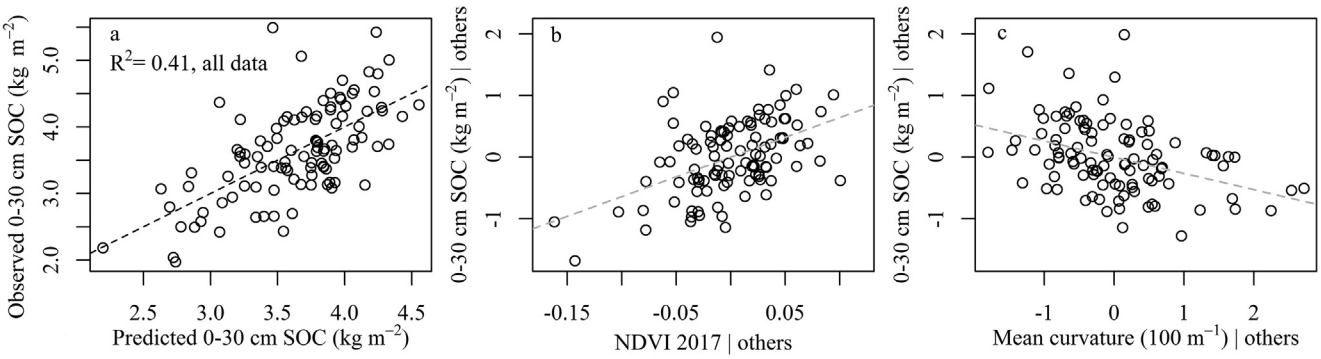

Fig. 4. a–c: Best two-variable model identified during cross-validation exercise, showing (a) Observed vs. predicted SOC and 1:1 line (black) and added-variable (aka 'partial regression') plots for each of the two predictors (x-axes) in this multiple linear regression best model: (b) mean growing season normalized difference vegetation index (NDVI) in 2017 and (c) mean curvature. Each partial regression plot shows the relative contribution of the predictor to explaining variance in SOC after accounting for the other predictor's explanatory power in the model. Gray lines show the best-fit for each partial regression plot. The slopes of these gray lines are equal to the explanatory variables' beta coefficients in the overall MLR model. The meaning of "| others" is "after accounting for the other predictor variables."

Table 6
Probability that observed spatial autocorrelation for a given soil property is random. Soil properties with p values < 0.05 all showed positive autocorrelation. SOC residuals are the model residuals from either the best performing two- or five-variable (var) multiple linear regression (MLR) model.

Soil property	0–30 cm	0–10 cm	10–30 cm
	p values		
SOC (%)	0.002	0.25	0.001
SOC (kg m^{-2})	0.001	0.02	0.001
Clay (%)	0.001	0.001	0.001
Sand (%)	0.001	0.001	0.001
Silt (%)	0.001	0.001	0.001
BD (g cm^{-3})	0.14	0.31	0.04
SOC residuals (two-var MLR)	0.13	0.23	0.25
SOC residuals (five-var MLR)	0.20	0.17	0.27

SOC = soil organic carbon; BD = bulk density.

contrasting growing seasons. This analysis showed a positive relationship between SOC and peak standing forage in both years, but the slope was steeper in the wet year (0.11 kg more forage kg^{-1} SOC m^{-2}). The relationship was statistically significant in 2017 (wet year; p = 0.02) when peak biomass was nearly three times higher than in 2018 (dry year) (Fig. S1).

4. Discussion

4.1. SOC patterns at catchment scale and relationship to topography and vegetation

Our study sought to contribute a catchment-scale perspective on SOC patterns by investigating a range of different microclimate and landscape position combinations in a semi-arid annual grassland. SOC stocks in the upper 30 cm showed strong evidence of spatial autocorrelation with a pattern directly related to elevation, curvature, and mean growing season NDVI from a wet year but not a dry year (Fig. 2; Tables 2 and 6). These direct relationships match intuitive expectations, such as more SOC in lower parts of the landscape where more vegetation is growing in a wet year (Figs. 1 and 5). The mechanism for SOC accretion in lower hillslope positions may differ from cultivated landscapes where erosion/deposition has been implicated in explaining landscape SOC distribution (Kirkels et al., 2014). At the hillslope scale in a 2-ha grassland in Southern California, Gessler et al. (2000) sampled soils on a SW-facing transect and reported that a Compound Topographic Index explained 78% of the variability in SOC stocks with more SOC in lower landscape positions. At our study site, additional forage production in a wet year was favored in concave locations, especially where soil moisture remained plentiful during a late season dry spell (Devine et al., 2019). This suggests that a wet year produces lateral redistribution of water and defines lower hillslope zones with surplus moisture where peak forage is produced and more SOC is accumulated over time, as indicated by higher NDVI (Fig. 1). Lower rainfall in the

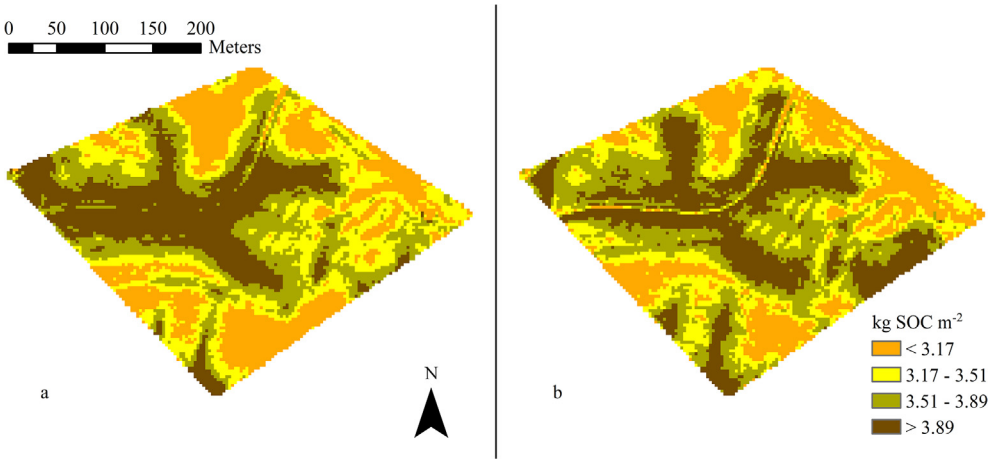

Fig. 5. a–b: Map of 0–30 cm soil organic carbon (SOC) produced from (a) best five-variable multiple linear regression model and (b) best two-variable multiple linear regression model. Class breaks are quartiles from the best five-variable multiple linear regression prediction.

dry year did not wet soil below 15 cm until late March, resulting in limited lateral water distribution. The dry-year NDVI pattern was unrelated to both wet-year NDVI and to SOC (Figs. 1 and 2; Table 2).

Linkages among wet-year NDVI, elevation, curvature, and SOC suggest that hillslope position and vegetation appear to be more important drivers of SOC patterns than aspect in central California semi-arid grasslands (Tables 2 and 4), even though insolation differences forced 3–10 °C soil temperature gradients in the catchment and noticeable differences in plant available moisture during wet-up periods (Devine et al., 2019). This lack of a clear, direct relationship between SOC and aspect is in contrast to several other catchment-scale studies. A SOC study in a rangeland catchment in Spain investigated patterns at a larger scale (2.7 km^2) and found that SOC stocks were generally lower in south-facing slopes with lower vegetative cover (Roman-Sanchez et al., 2018). Similarly, in Idaho along a nearly 1-km elevation gradient spanning both grassland and forested sites on different aspects, insolation and NDVI accounted for 62% of SOC variability with north-facing slopes having up to 5 times the SOC stock in the lower elevation sites of the watershed compared to south-facing slopes (Kunkel et al., 2011). In contrast, in semi-arid rangelands of Australia, no significant relationship was reported between aspect and SOC, while elevation, precipitation, and vegetation indices were linked to SOC patterns and explained nearly half of regional variability (Wang et al., 2018a). In summary, soil moisture and productivity appears more related to SOC gradients in this semi-arid catchment than soil temperature.

4.2. Modeling SOC stocks at catchment scale: a climate change and regional scale perspective

At first glance, the parameter coefficient estimates from the best MLR model (five variables) suggest that aspect (via insolation) is the most important variable (Table 4), in direct contradiction to the conclusion drawn from the univariate tests (Table 2). MLR parameter estimates from the best model make intuitive sense with more SOC where there is higher productivity in a wet year, concave compared to convex landforms, downslope positions, gentler slopes, and on cooler aspects (Table 4). However, the five-variable model was an improvement of only 8.3% in cross-validated RMSE (0.04 kg m^{-2}) compared to a more parsimonious, two-variable model that used only curvature and wet-year NDVI and explained 41% of 0–30 cm SOC variance (Table 4; Figs. 3 and 4). Inference from the five-variable model should be tempered by marginal improvement in explained variance and by four other model inferences. First, collinearity between slope and insolation is undermining reliable coefficient estimates. When slope and insolation were included together in the five-variable model, it more than doubled the coefficient estimate for insolation compared to coefficient estimates derived from the best three- and four-variable MLR models that included insolation but did not include the collinear slope (Table 4). Second, while the best three- and four-variable MLR models included insolation, these models showed very small improvements over the two-variable model (Table 4). Third, the best random forest model did not include insolation (Table 4). Fourth, post-hoc variable importance metrics supported these modeling observations, suggesting that wet-year NDVI and curvature were responsible for 70% of the explained variance in the five-variable model. In summary, while the conceptual model of annual rangeland production in California typically conceives of a landscape where south-facing aspects are deficient in soil moisture thereby constraining forage growth (Becchetti et al., 2016), SOC patterns from this analysis suggest that southern exposures may have only marginally less SOC storage compared to northern exposures.

There are unresolved questions related to how climate change will impact annual range production and SOC stocks in complex topography. Warmer temperatures and greater insolation on south-facing slopes can enhance winter forage growth during wet years in California annual rangelands (Devine et al., 2019; Evans et al., 1975), and this may partly compensate for the negative effect that enhanced drying has on forage growth and its feedback to SOC. However, mid-winter droughts can also sharply impact growth on south-facing aspects (Devine et al., 2019). Studies have reported either negative or no association between warmer southern aspects and forage productivity at the Jasper Ridge rangeland study site in California (McNaughton, 1968), where a soil warming experiment also did not boost forage growth (Dukes et al., 2005; Zhu et al., 2016). In addition, warmer soil temperatures would be expected to favor more rapid microbial decomposition of residual forage and SOC. Thus, the future of climate change suggests a mixed signal for SOC stocks in the complex topography of California annual rangelands where patterns in productivity may change with warmer winters and more pronounced precipitation volatility, forcing new steady-state SOC patterns.

Our cross-validation results, while modest with an R^2 of 0.44 for the best 0–30 cm SOC MLR model (Table 5), are still at the high end compared to digital SOC mapping at similar scales and in comparable landscapes. A Mediterranean rangeland study at a slightly larger extent (2.7 km^2) in Spain explained 18% of variability in validation data using a similar but larger set of predictors and a Random Forest modeling approach (Roman-Sanchez et al., 2018). In eastern semi-arid Australia, Random Forest and boosted regression tree approaches explained 42–48% of validation set 0–30 cm SOC variation starting from a set of 28 environmental covariates (Wang et al., 2018a). At an even larger scale in this Australian region, these same two statistical approaches and Support Vector Machines explained, on average, 48% of 0–30 cm SOC variation with a smaller set of environmental covariates (Wang et al., 2018b). Covering 8118 ha and spanning forest and vineyard land uses, a study from Brazil reported validation R^2 values of 0.33–0.44 for five different soil depth intervals (Bonfatti et al., 2016).

Like our study, Bonfatti et al. (2016) demonstrated MLR models outperformed Random Forest modeling of SOC in five different soil depth intervals. Indeed, when predictors have linear relationships with a response variable (Figs. 2 and 3), it is acknowledged (but perhaps not well appreciated) that simpler modeling approaches such as MLR can outperform more complex modeling approaches such as Random Forest (James et al., 2013). Moreover, similar to our results, Bonfatti et al. (2016) found no autocorrelation in MLR residuals, meaning there was no additional advantage for employing a regression kriging technique for mapping SOC (Keskin and Grunwald, 2018).

In our study, while there was a coherent relationship between 0-30 cm SOC and terrain attributes, the less clear relationship between 0-10 cm SOC and terrain attributes highlights the inability of digital soil mapping techniques to unequivocally work well everywhere (Tables 2, 5, and S1). The relative noisiness of the 0–10 cm layer compared to the 10–30 cm layer was intriguing and could be attributed to at least four mechanisms. First, erosion/deposition processes may not be at steady-state in the catchment. While no evidence of overland flow was observed in field campaigns, lack of vegetative cover during severe droughts makes soils susceptible both to wind and water erosion. Alternatively, dynamic forage productivity patterns on the landscape may be forcing surficial SOC to a new steady state. Additionally, selective grazing by cattle may create patchiness in residual dry matter which could influence SOC patterns as plant material decomposes (Roman-Sanchez et al., 2018). Finally, burrowing fauna such as ground squirrels and pocket gophers may create SOC patchiness through bioturbation.

There is a lack of testing assumptions concerning SOC patterns at the catchment scale in uncultivated landscapes in spite of the common acknowledgement that SOC is expected to vary with topography, microclimate, and vegetation at fine resolutions (Minasny et al., 2013). Moreover, catchment scale SOC patterns may not match regional scale SOC trends with the same variables, such as elevation, where increasing elevation is often associated with more SOC (Post et al., 1982), the opposite of what we observed at the catchment scale and others have observed at hillslope scale (Gessler et al., 2000). Positive relationships between SOC and either precipitation or elevation (acting as proxies for increased biomass and cooler temperatures that hinder decomposition)

at regional scales have been documented in complex terrain in Mediterranean climates in both California and Australia (Jenny et al. 1968; Dahlgren et al., 1997a; Rasmussen et al., 2007; 2010; Kunkel et al., 2019). Silver et al. (2010) did not find a significant relationship between 0-30 cm SOC stocks and either precipitation or temperature in a *meta*-analysis of California rangeland soils (n = 39), perhaps because variable mineralogy across these study sites has an overshadowing influence on SOC stabilization. There is clearly a need for further development of SOC mapping approaches that fuse both regional and catchment scale understanding with recognition that digital mapping techniques may only work in particular landscapes (Beaudette and O'Geen, 2016). Such efforts could produce fine-resolution estimates of SOC at the catchment scale that also reflect regional-scale trends and soil forming factors spanning multiple vegetation, climate, and soil types.

5. Conclusion

We found correspondence of SOC to soil forming factors, principally topography, organisms (vegetation), and (micro-)climate at the catchment scale in a Central Coast annual grassland of California. Overall, MLR modeling results showed fine-scale terrain properties can be more useful predictors of SOC stocks than measured values at nearby points. How much vegetation is growing in a particular location (as indicated by remotely sensed "greenness") and terrain curvature explained most SOC variation, but there was also a smaller but significant relationship to aspect, slope, and elevation revealed while accounting for these two covariates. The negative relationship with south-facing aspects (drier and less productive) was weaker than expected given prior studies and our landscape preconceptions. These relationships deserve further exploration in other semi-arid rangeland catchments. This study demonstrates promise for improving regional carbon accounting in complex terrain using fine resolution digital surface models and remote sensing.

Declaration of Competing Interest

The authors declare that they have no known competing financial interests or personal relationships that could have appeared to influence the work reported in this paper.

Acknowledgements

We thank Tad Doane for sharing his analytical expertise and Yanxu Yao and Jennifer Martin for their assistance in the lab. This work was supported by the Russell L. Rustici Rangeland and Cattle Research Endowment and Henry A. Jastro Graduate Research Award.

Appendix A. Supplementary data

Supplementary data to this article can be found online at https://doi.org/10.1016/j.geoderma.2020.114286.

References

Batjes, N.H., 2016. Harmonized soil property values for broad-scale modelling (WISE30sec) with estimates of global soil carbon stocks. Geoderma 269, 61–68. https://doi.org/10.1016/j.geoderma.2016.01.034.

Beaudette, D.E., O'Geen, A.T., 2016. Topographic and geologic controls on soil variability in California's Sierra Nevada foothill region. Soil Sci. Soc. Am. J. 80, 341–354. https://doi.org/10.2136/sssaj2015.07.0251.

Becchetti, T., George, M., McDougald, N., Dudley, D., Connor, M., Flavel, D., Vaughn, C., Forero, L., Frost, B., Larsen, R., Striby, K., Davy, J., Doran, M., Markegard, D., 2016. Rangeland Management Series: Annual Range Forage Production, ANR Publication 8018. University of California Agriculture and Natural Resources, Richmond, CA.

Bivand, R.S., Wong, D.W.S., 2018. Comparing implementations of global and local indicators of spatial association. Test 27, 716–748. https://doi.org/10.1007/s11749-018-0599-x.

Bonfatti, B.R., Hartemink, A.E., Giasson, E., Tornquist, C.G., Adhikari, K., 2016. Digital mapping of soil carbon in a viticultural region of Southern Brazil. Geoderma 261, 204–221. https://doi.org/10.1016/j.geoderma.2015.07.016.

Dahlgren, R.A., Boettinger, J.L., Huntington, G.L., Amundson, R.G., 1997a. Soil development along an elevational transect in the western Sierra Nevada, California. Geoderma 78, 207–236. https://doi.org/10.1016/S0016-7061(97)00034-7.

Dahlgren, R.A., Singer, M.J., Huang, X., 1997b. Oak tree and grazing impacts on soil properties and nutrients in a California oak woodland. Biogeochemistry 39, 45–64. https://doi.org/10.1023/A:1005812621312.

Daly, C., Halbleib, M., Smith, J.I., Gibson, W.P., Doggett, M.K., Taylor, G.H., Curtis, J., Pasteris, P.P., 2008. Physiographically sensitive mapping of climatological temperature and precipitation across the conterminous United States. Int. J. Climatol. 28, 2031–2064. https://doi.org/10.1002/joc.1688.

Dane, J.H., Topp, G.C., 2002. Methods of Soil Analysis: Physical Methods, Part 4. Soil Science Society of America Inc, Madison, WI.

Devine, S.M., O'Geen, A.T., Larsen, R.E., Dahlke, H.E., Liu, H., Jin, Y., Dahlgren, R.A., 2019. Microclimate–forage growth linkages across two strongly contrasting precipitation years in a Mediterranean catchment. Ecohydrology 12 (8). https://doi.org/10.1002/eco.v12.810.1002/eco.2156.

Domke, G.M., Perry, C.H., Walters, B.F., Nave, L.E., Woodall, C.W., Swanston, C.W., 2017. Toward inventory-based estimates of soil organic carbon in forests of the United States. Ecol. Appl. 27, 1223–1235. https://doi.org/10.1002/eap.1516.

Dukes, J.S., Chiariello, N.R., Cleland, E.E., Moore, L.A., Shaw, M.R., Thayer, S., Tobeck, T., Mooney, H.A., Field, C.B., 2005. Responses of grassland production to single and multiple global environmental changes. PLoS Biol. 3, e319. https://doi.org/10.1371/journal.pbio.0030319.

Evans, R.A., Kay, B.L., Young, J.A., 1975. Microenvironment of a dynamic annual community in relation to range improvement. Hilgardia 43 (3), 79–102. https://doi.org/10.3733/hilg.v43n03p079.

Fox, J., Weisberg, S., 2011. An R Companion to Applied Regression, second ed. Sage, Thousand Oaks, CA.

FRAP, 2018. California's Forests and Rangelands: 2017 Assessment. California Department of Forestry and Fire Protection, Fire Resource and Assessment Program, Sacramento, CA. http://frap.fire.ca.gov/assessment2017/FinalAssessment2017/Assessment2017.pdf (accessed 2 August 2018).

Galbraith, J.M., Kleinman, P.J.A., Bryant, R.B., 2003. Sources of uncertainty affecting soil organic carbon estimates in northern New York. Soil Sci. Soc. Am. J. 67, 1206–1212. https://doi.org/10.2136/sssaj2003.1206.

Gavlak, R., Horneck, D., Miller, R., 2005. Plant, Soil and Water Reference Methods for the Western Region, third ed. Western Rural Development Center, Corvallis, OR.

Gessler, P.E., Chadwick, O.A., Chamran, F., Althouse, L., Holmes, K., 2000. Modeling soil-landscape and ecosystem properties using terrain attributes. Soil Sci. Soc. Am. J. 64, 2046–2056. https://doi.org/10.2136/sssaj2000.6462046x.

Gordon, D.R., Rice, K.J., 1992. Partitioning of space and water between two California annual grassland species. Am. J. Bot. 79, 967–976. https://doi.org/10.1002/j.1537-2197.1992.tb13685.x.

Graler, B., Pebesma, E., Heuvelink, G., 2016. Spatio-temporal interpolation using gstat. R J. 8, 204-218. https://doi.org/10.32614/RJ-2016-014.

Groemping, U., 2006. Relative importance for linear regression in R: the package relaimpo. J. Stat. Software 17 (1). https://doi.org/10.18637/jss.v017.i01.

Hancock, G.R., Murphy, D., Evans, K.G., 2010. Hillslope and catchment scale soil organic carbon concentration: An assessment of the role of geomorphology and soil erosion in an undisturbed environment. Geoderma 155, 36–45. https://doi.org/10.1016/j.geoderma.2009.11.021.

Hijmans, R.J., 2017. Raster: Geographic Data Analysis and Modeling. R package version 2.6-7. https://CRAN.R-project.org/package=raster.

Holmes, T.H., Rice, K.J., 1996. Patterns of growth and soil-water utilization in some exotic annuals and native perennial bunchgrasses of California. Ann. Bot. 78, 233–243. https://doi.org/10.1006/anbo.1996.0117.

Homann, P.S., Sollins, P., Fiorella, M., Thorson, T., Kern, J.S., 1998. Regional soil organic carbon storage estimates for western Oregon by multiple approaches. Soil Sci. Soc. Am. J. 62, 789–796. https://doi.org/10.2136/sssaj1998.03615995006200030036x.

James, G., Witten, D., Hastie, T., Tibshirani, R., 2013. Introduction to Statistical Learning: with Applications in R. Springer, New York https://doi.org/10.1007/978-1-4614-7138-7.

Jenny, H., Salem, A.E., Wallis, J.R., 1968. Interplay of soil organic matter and soil fertility with state factors and soil properties. In: Salviucci, P. (Ed.), Study Week on Organic Matter and Soil Fertility. John Wiley and Sons Inc, New York, NY, pp. 5–37.

Keskin, H., Grunwald, S., 2018. Regression kriging as a workhorse in the digital soil mapper's toolbox. Geoderma 326, 22–41. https://doi.org/10.1016/j.geoderma.2018.04.004.

Kirkels, F., Cammeraat, L.H., Kuhn, N.J., 2014. The fate of soil organic carbon upon erosion, transport and deposition in agricultural landscapes – a review of different concepts. Geomorphology 226, 94–105. https://doi.org/10.1016/j.geomorph.2014.07.023.

Kunkel, M.L., Flores, A.N., Smith, T.J., McNamara, J.P., Benner, S.G., 2011. A simplified approach for estimating soil carbon and nitrogen stocks in semi-arid complex terrain. Geoderma 165, 1–11. https://doi.org/10.1016/j.geoderma.2011.06.011.

Kunkel, V., Hancock, G.R., Wells, T., 2019. Large catchment-scale spatiotemporal distribution of soil organic carbon. Geoderma 334, 175–185. https://doi.org/10.1016/j.geoderma.2018.07.046.

Larsen, R., Striby, K., Horney, M., 2014. Fourteen years of forage monitoring on the California Central Coast shows tremendous variation. In: Standiford, R.B., Purcell, K. L. (Eds.), Proceedings of the 7th California Oak Symposium: Managing Oak Woodlands in a Dynamic World, Gen. Tech. Rep. PSW-GTR-251. U.S.D.A., Forest Service, Pacific Southwest Research Station, Berkeley, CA, pp. 273–281.

Liaw, A., Wiener, M., 2002. Classification and regression by randomForest. R News 2(3), 18-22. https://cran.r-project.org/doc/Rnews/Rnews_2002-3.pdf (accessed 17 March

2019).
Liu, H., Dahlgren, R.A., Larsen, R.E., Devine, S.M., Roche, L.M., O'Geen, A.T., Wong, A.J.Y., Covello, S., Jin, Y., 2019. Estimating rangeland forage production using remote sensing data from a small unmanned aerial system (sUAS) and PlanetScope satellite. Remote Sens. 11 (5), 595. https://doi.org/10.3390/rs11050595.
McNaughton, S.J., 1968. Structure and function in California grasslands. Ecol. 49, 962–972. https://doi.org/10.2307/1936547.
Midwood, A.J., Boutton, T.W., 1998. Soil carbonate decomposition by acid has little effect on delta C-13 of organic matter. Soil Biol. Biochem. 30, 1301–1307. https://doi.org/10.1016/S0038-0717(98)00030-3.
Minasny, B., McBratney, A.B., Malone, B.P., Wheeler, I., 2013. Digital mapping of soil carbon. Adv. Agron. 118, 1–47. https://doi.org/10.1016/B978-0-12-405942-9.00001-3.
Pebesma, E.J., 2004. Multivariable geostatistics in S: the gstat package. Comput. Geosci. 30, 683–691. https://doi.org/10.1016/j.cageo.2004.03.012.
Pennock, D.J., Anderson, D.W., Dejong, E., 1994. Landscape-scale changes in indicators of soil quality due to cultivation in Saskatchewan, Canada. Geoderma 64, 1–19. https://doi.org/10.1016/0016-7061(94)90086-8.
Post, W.M., Emanuel, W.R., Zinke, P.J., Stangenberger, A.G., 1982. Soil carbon pools and world life zones. Nature 298, 156–159. https://doi.org/10.1038/298156a0.
Core Team, R., 2018. R: A Language and Environment for Statistical Computing. R Foundation for Statistical Computing, Vienna, Austria.
Rasmussen, C., Dahlgren, R.A., Southard, R.J., 2010. Basalt weathering and pedogenesis across an environmental gradient in the southern Cascade Range, California, USA. Geoderma 154, 473–485. https://doi.org/10.1016/j.geoderma.2009.05.019.
Rasmussen, C., Matsuyama, N., Dahlgren, R.A., Southard, R.J., Brauer, N., 2007. Soil genesis and mineral transformation across an environmental gradient on andesitic lahar. Soil Sci. Soc. Am. J. 71, 225–237. https://doi.org/10.2136/sssaj2006.0100.
Ratliff, R.D., Frost, W.E., 1990. Estimating botanical composition by the dry-weight-rank method in California's annual grasslands. Research Note PSW-410. U.S.D.A., Forest Service, Pacific Southwest Research Station, Berkeley, CA.
Roman-Sanchez, A., Vanwalleghem, T., Pena, A., Laguna, A., Giraldez, J.V., 2018. Controls on soil carbon storage from topography and vegetation in a rocky, semi-arid landscapes. Geoderma 311, 159–166. https://doi.org/10.1016/j.geoderma.2016.10.013.
Salls, W.B., Larsen, R.E., Lewis, D.J., Roche, L.M., Eastburn, D.J., Hollander, A.D., Walkinshaw, M., Kaffka, S.R., Tate, K.W., O'Geen, A.T., 2018. Modeled soil erosion potential is low across California's annual rangelands. Calif. Agric. 72, 179–191. https://doi.org/10.3733/ca.2018a0021.
Silver, W.L., Ryals, R., Eviner, E., 2010. Soil carbon pools in California's annual grassland ecosystems. Rangeland Ecol. Manage. 63, 128–136. https://doi.org/10.2111/REM-D-09-00106.1.
Soil Science Division Staff, 2017. Soil Survey Manual. Ditzler, C., Scheffe, K., Monger, H. C. (Eds.) U.S.D.A. Handbook 18. U.S. Government Printing Office, Washington D.C.
Soil Survey Staff. 2003. Soil Survey of San Luis Obispo County, California, Carrizo Plain Area. U.S.D.A., Natural Resources Conservation Service, National Cooperative Soil Survey.
Suddick, E.C., Ngugi, M.K., Paustian, K., Six, J., 2013. Monitoring soil carbon will prepare growers for a carbon trading system. Calif. Agric. 67, 162–171. https://doi.org/10.3733/ca.v067n03p162.
Thompson, J.A., Kolka, R.K., 2005. Soil carbon storage estimation in a forested watershed using quantitative soil-landscape modeling. Soil Sci. Soc. Am. J. 69, 1086–1093. https://doi.org/10.2136/sssaj2004.0322.
Wang, B., Waters, C., Orgill, S., Cowie, A., Clark, A., Liu, D., Simpson, M., McGowen, I., Sides, T., 2018a. Estimating soil organic carbon stocks using different modelling techniques in the semi-arid rangelands of eastern Australia. Ecol. Indic. 88, 425–438. https://doi.org/10.1016/j.ecolind.2018.01.049.
Wang, B., Waters, C., Orgill, S., Gray, J., Cowie, A., Clark, A., Liu, D.L., 2018b. High resolution mapping of soil organic carbon stocks using remote sensing variables in the semi-arid rangelands of eastern Australia. Sci. Total Environ. 630, 367–378. https://doi.org/10.1016/j.scitotenv.2018.02.204.
Zhu, K., Chiariello, N.R., Tobeck, T., Fukami, T., Field, C.B., 2016. Nonlinear, interacting responses to climate limit grassland production under global change. Proc. Natl. Acad. Sci. U.S.A. 113, 10589–10594. https://doi.org/10.1073/pnas.1606734113.